Supporting Information

Manganese vanadium oxide –N-doped reduced graphene oxide composites as oxygen reduction and oxygen evolution electrocatalysts

*Xiaolin Xing,[a‡] Rongji Liu,[*a,b‡] Kecheng Cao,[d] Ute Kaiser,[c,d] Guangjin Zhang[b] and Carsten Streb[*a,c]*

[a]Ulm University, Institute of Inorganic Chemistry I, Albert-Einstein-Allee 11, 89081 Ulm, Germany

[b]Key Laboratory of Green Process and Engineering, Institute of Process Engineering, Chinese Academy of Sciences, 100190, Beijing, China

[c]Helmholtz-Institute Ulm for Electrochemical Energy Conversion, Helmholtzstr. 11, 89081 Ulm, Germany

[d]Central Facility of Electron Microscopy for Materials Science, Ulm University, 89081 Ulm, Germany

‡ These authors contributed equally to this work

*Emails: carsten.streb@uni-ulm.de (Carsten Streb), rongji.liu@uni-ulm.de (Rongji Liu)

1. Calculations for Electrochemical Studies

In order to further investigate the selectivity of oxygen reduction for a four-electron pathway, Koutecky−Levich plots (J^{-1} vs. $\omega^{-1/2}$) were analyzed at different potentials. The slopes of their best linear fit lines were used to calculate the number of electrons transferred (n) according to the Koutecky−Levich equation [1]

$$\frac{1}{J} = \frac{1}{J_L} + \frac{1}{J_K} = \frac{1}{B\omega^{1/2}} + \frac{1}{J_K}$$

$$B = 0.62nFC_0D_0^{2/3}\nu^{-1/6}\ ;\ J_K = nFkC_0$$

Where J is the measured current density, J_K and J_L are the kinetic and diffusion limiting current densities, ω is the angular velocity, n is transferred electron number, F is the

Faraday constant, C_0 is the bulk concentration of O_2, ν is the kinematic viscosity of the electrolyte, and k is the electron-transfer rate constant.

The yield of peroxides (HO_2^-%) and the electron transfer number (n) were calculated by the followed equation [2]

$$\mathrm{HO_2^-} = 200\frac{I_r/N}{I_d + I_r/N}$$

$$n = 4\frac{I_r/N}{I_d + I_r/N}$$

Where I_d is disk current, I_r is ring current, and N is current collection efficiency of the Pt ring. N was calibrated as 0.40 on the basis of the ORR measurements of $K_3Fe[CN]_6$.

2. High-resolution transmission electron microscopy (HRTEM)

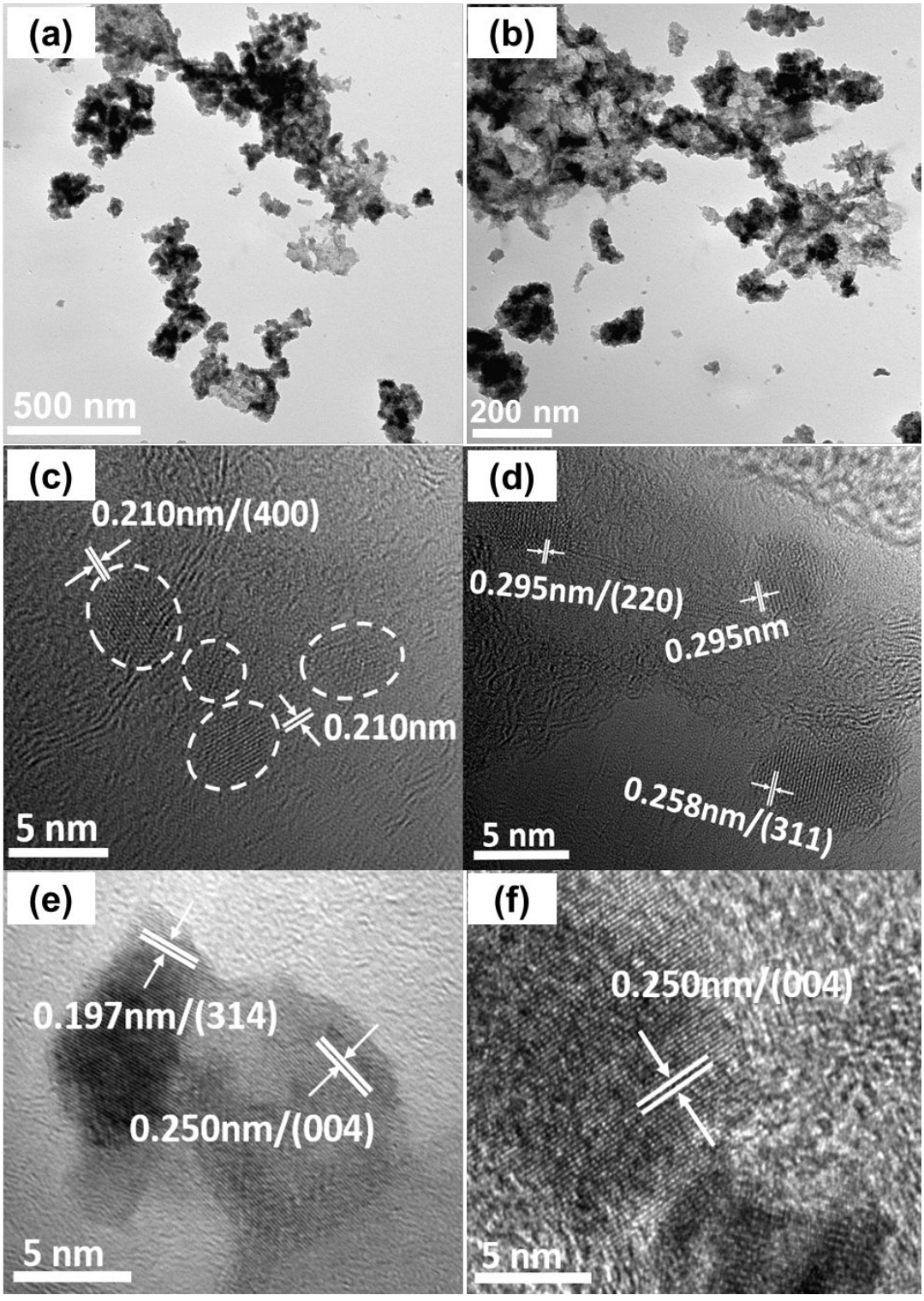
(a)
500 nm
(b)
200 nm
(c)
0.210nm/(400)
0.210nm
5 nm
(d)
0.295nm/(220)
0.295nm
0.258nm/(311)
5 nm
(e)
0.197nm/(314)
0.250nm/(004)
5 nm
(f)
0.250nm/(004)
5 nm

Figure S1. TEM images of native $\{Mn_4V_4\}$ (a and b). HRTEM images of (c and d) **1-900** and (e and f) **1-440**, showing the lattice fringes of crystalline manganese vanadium oxide particles deposited on N-rGO.

3. X-ray photoelectron spectroscopy (XPS)

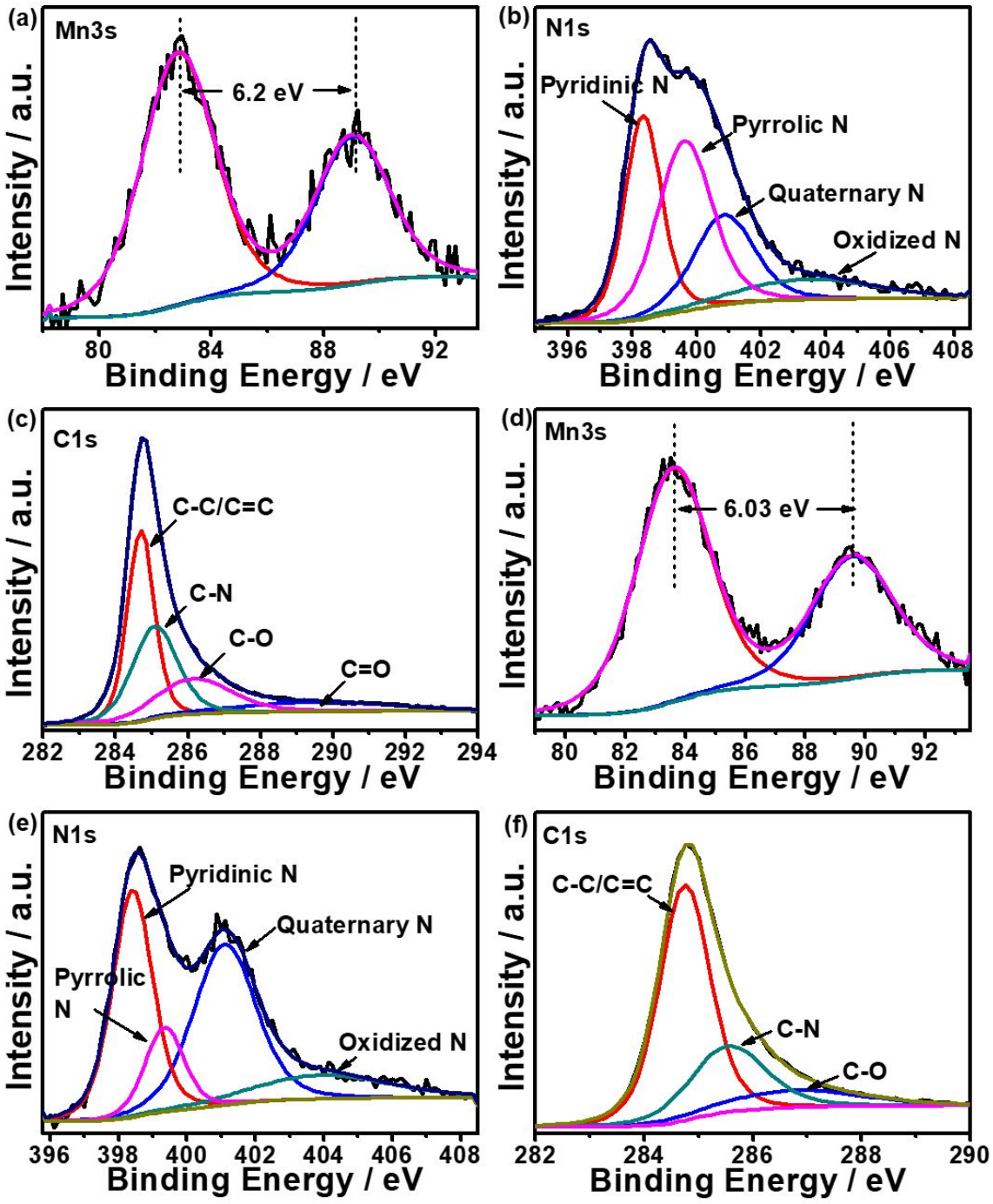

Figure S2. Manganese, nitrogen and carbon XPS spectra for **1-440** (a, b, c) and **1-900** (d, e, f).

4. Linear scan voltammograms (LSV)

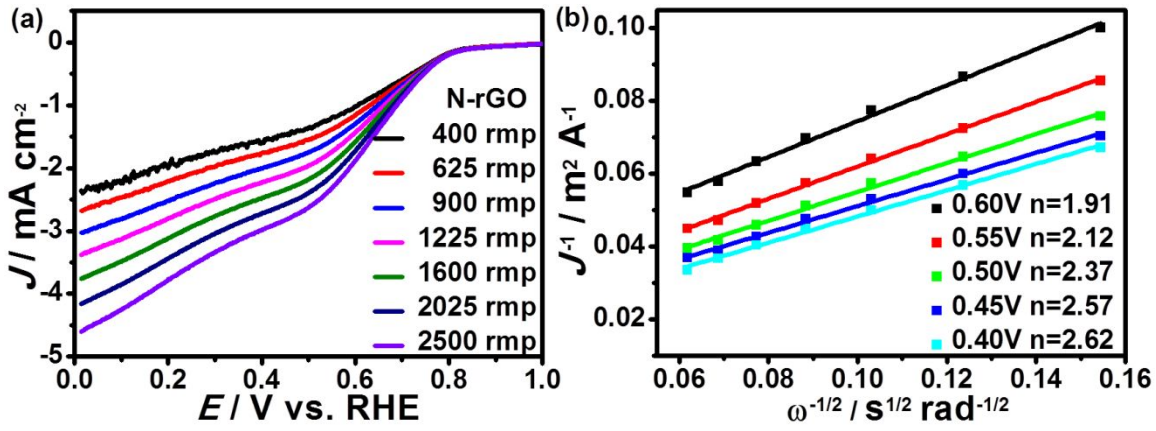

Figure S3. Linear sweep voltammograms (LSV) recorded by RDE in O_2 saturated 0.1 M aqueous KOH solution at different rotation rates for non-modified N-rGO (a); (b) shows the Koutecky–Levich plots of J^{-1} versus $\omega^{-1/2}$ at different electrode potentials for the corresponding material N-rGO.

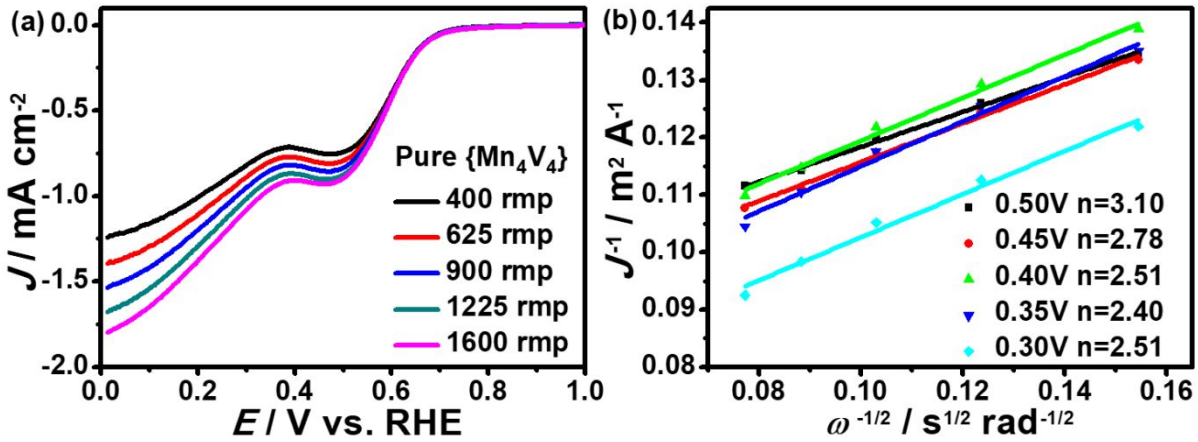

Figure S4. Linear sweep voltammograms (LSV) recorded by RDE in O_2 saturated 0.1 M aqueous KOH solution at different rotation rates for native $\{Mn_4V_4\}$ (a); (b) shows the

Koutecky–Levich plots of J^{-1} versus $\omega^{-1/2}$ at different electrode potentials for the corresponding material $\{Mn_4V_4\}$.

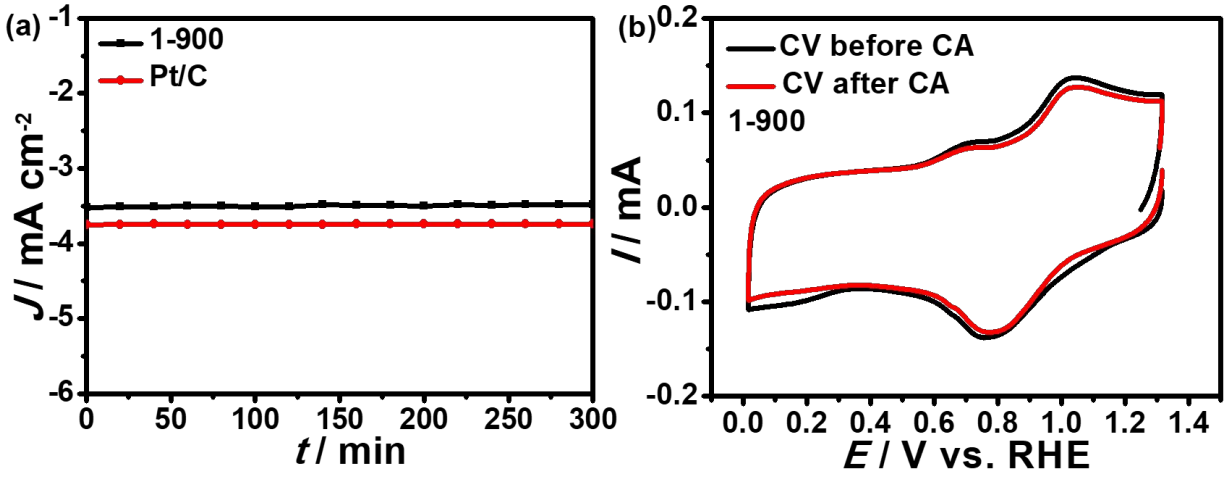

Figure S5. (a) Chronoamperometry (CA) tests of **1-900** and commercial Pt/C, demonstrating their stability during ORR. Conditions: E = 0.7 V, 0.1 M aqueous KOH as electrolyte. (b) CVs of **1-900** before and after stability test, scan rate: 10 mV s^{-1}.

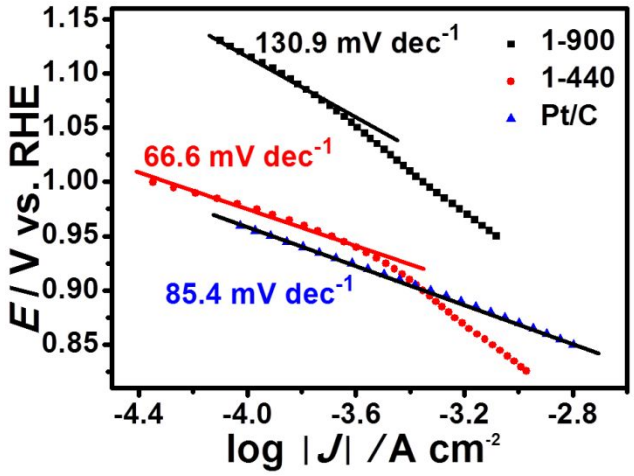

Figure S6. Tafel plots (derived from Fig. 5a) of **1-900**, **1-440** and commercial Pt/C for ORR in 0. 1 M aqueous KOH solution.

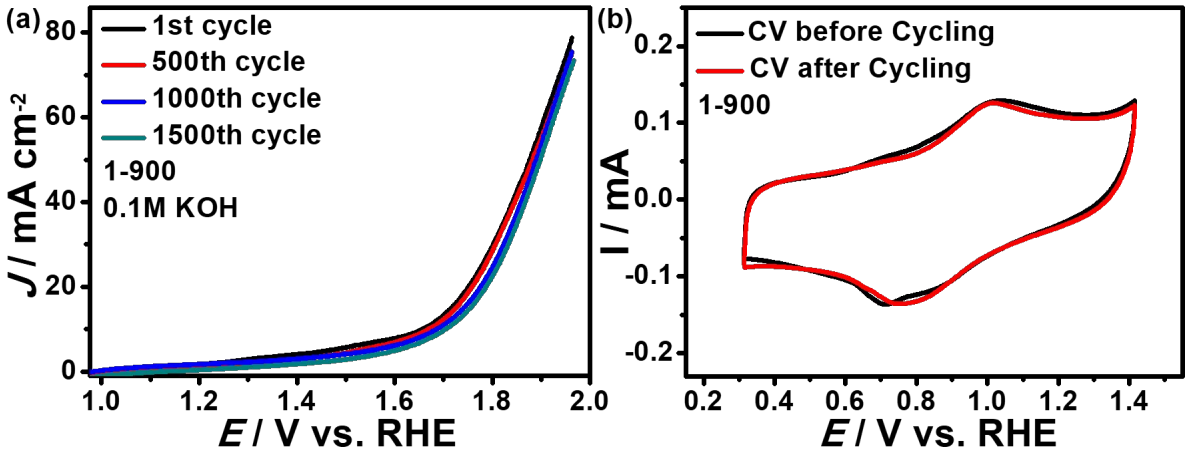

Figure S7. (a) Linear sweep voltammograms (LSV) of **1-900** before and after different cycles of accelerated stability test in O_2-saturated 0.1 M KOH. (b) CVs before and after stability test. Catalyst loading amount: ~1 mg cm^{-2} on carbon fiber paper. Sweep rate: 10 mV s^{-1}.

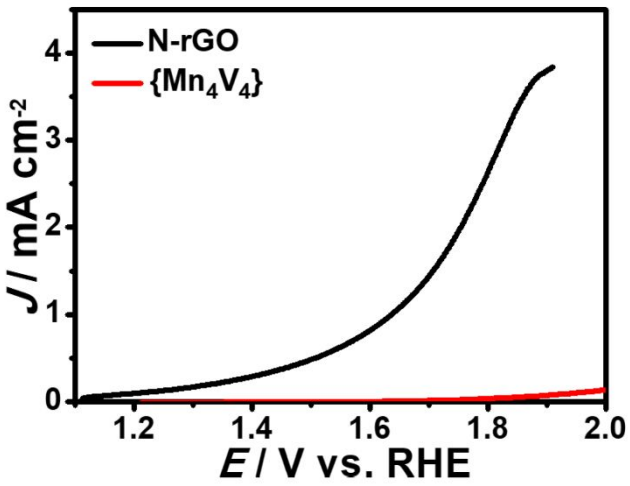

Figure S8. Linear sweep voltammograms (LSV) of N-rGO and native $\{Mn_4V_4\}$ in 0.1M KOH. The LSV was measured in O_2-saturated solution with a scan rate of 10 mV s^{-1} and catalyst loading of 1 mg cm^{-2} on carbon fiber paper.

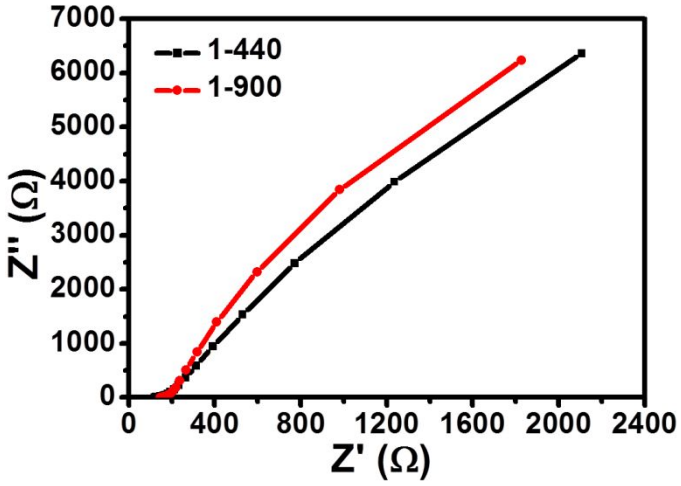

Figure S9. Electrochemical impedance spectra (EIS) curves in 0.1 M KOH for 1-440 and 1-900.

Table S1 Electrocatalytic data for related catalytic systems

Catalyst	$E_{onset\ (ORR)}$ (V vs. RHE)	E_{ORR} (V vs. RHE)	E_{OER} (V vs. RHE)	$\Delta E_{OER-ORR}$(V)	Reference
20 wt % Pt /C		0.86	2.02	1.16	[3]
20 wt % Ir /C		0.69	1.61	0.92	[3]
20 wt % Ru/C		0.61	1.62	1.01	[3]
NPMC-1000	0.94	0.85	~1.95	1.1	[4]
NGSH	0.88	~0.63	~1.64	1.01	[5]
CNT@NCNT	0.99	0.632	1.762	1.13	[6]
N-graphene-CNT	0.884	0.684	1.65	0.966	[7]
PCN-CFP	0.94	0.67	1.63	0.96	[8]
Co/N-C	0.834	-	-	0.859	[9]
CMO-20N-rGO	0.93	0.77	1.68	0.91	[10]
$NiCo_2O_4$-G	0.892	0.612	~1.692(CV)	1.080	[11]
$NiCo_2S_4$@S-rGO	-0.08 vs.Ag/AgCl	-0.24 vs.Ag/AgCl	0.7 vs.Ag/AgCl	0.94	[12]
$CoFe_2O_4$@rGO	0.841	~0.747	~1.707	0.96	[13]

$CoMn_2O_4$@N-rGO	0.9	0.8	1.66	0.86	[14]
$nsLaNiO_3$@NC	-	0.64	1.66	1.02	[15]

$E_{onset\ (ORR)}$, onset potential for ORR; E_{ORR}, potential for ORR at J = -3 mA cm^{-2}; E_{OER}, potential for OER at J = 10 mA cm^{-2}.

$E_{RHE} = E_{Ag/AgCl} + E^{\circ}_{Ag/AgCl} + 0.059\ pH$

$E_{RHE} = E_{SCE} + E^{\circ}_{SCE} + 0.059\ pH$

where E_{RHE} is the converted potential vs RHE; $E_{Ag/AgCl}$, and E_{SCE} are the experimental potentials measured against Ag/AgCl and SCE reference electrodes, respectively; $E^{\circ}_{Ag/AgCl}$ and E°_{SCE} are the standard potential of Ag/AgCl and SCE at 25 °C, respectively.

References

(1) Paulus, U. A.; Schmidt, T. J.; Gasteiger, H. A.; Behm, R. J. Oxygen Reduction on a High-Surface Area Pt/Vulcan Carbon Catalyst: A Thin-Film Rotating Ring-Disk Electrode Study. *J. Electroanal. Chem.* **2001**, *495*, 134–145.

(2) Hao, L.; Zhang, S.; Liu, R.; Ning, J.; Zhang, G.; Zhi, L. Bottom-up Construction of Triazine-Based Frameworks as Metal-Free Electrocatalysts for Oxygen Reduction Reaction. *Adv. Mater.* **2015**, *27*, 3190–3195.

(3) Gorlin, Y.; Lassalle-Kaiser, B.; Benck, J. D.; Gul, S.; Webb, S. M.; Yachandra, V. K.; Yano, J.; Jaramillo, T. F. In Situ X-Ray Absorption Spectroscopy Investigation of a Bifunctional Manganese Oxide Catalyst with High Activity for Electrochemical Water Oxidation and Oxygen Reduction. *J. Am. Chem. Soc.* **2013**, *135*, 8525–8534.

(4) Zhang, J.; Zhao, Z.; Xia, Z.; Dai, L. A Metal-Free Bifunctional Electrocatalyst for Oxygen Reduction and Oxygen Evolution Reactions. *Nat. Nanotechnol*. 2015, *10*, 444–452.

(5) Tian, G. L.; Zhao, M. Q.; Yu, D.; Kong, X. Y.; Huang, J. Q.; Zhang, Q.; Wei, F. Nitrogen-Doped Graphene/Carbon Nanotube Hybrids: In Situ Formation on Bifunctional Catalysts and Their Superior Electrocatalytic Activity for Oxygen Evolution/Reduction Reaction. *Small* **2014**, *10*, 2251–2259.

(6) Tian, G. L.; Zhang, Q.; Zhang, B.; Jin, Y. G.; Huang, J. Q.; Su, D. S.; Wei, F. Toward Full Exposure of "Active Sites": Nanocarbon Electrocatalyst with Surface Enriched Nitrogen for Superior Oxygen Reduction and Evolution Reactivity. *Adv. Funct. Mater.* **2014**, *24*, 5956–5961.

(7) Wen, Z.; Ci, S.; Hou, Y.; Chen, J. Facile One-Pot, One-Step Synthesis of a Carbon Nanoarchitecture for an Advanced Multifunctonal Electrocatalyst. *Angew. Chem. Int. Ed*. 2014, *53*, 6496–6500.

(8) Ma, T. Y.; Ran, J.; Dai, S.; Jaroniec, M.; Qiao, S. Z. Phosphorus-Doped Graphitic Carbon Nitrides Grown In Situ on Carbon-Fiber Paper: Flexible and Reversible Oxygen Electrodes. *Angew. Chem. Int. Ed.* **2015**, *54*, 4646–4650.

(9) Su, Y.; Zhu, Y.; Jiang, H.; Shen, J.; Yang, X.; Zou, W.; Chen, J.; Li, C. Cobalt Nanoparticles Embedded in N-Doped Carbon as an Efficient Bifunctional

Electrocatalyst for Oxygen Reduction and Evolution Reactions. *Nanoscale* **2014**, *6*, 15080–15089.

(10) He, X.; Yin, F.; Yuan, S.; Liu, N.; Huang, X. Hybrid Spinel Oxides/N-Doped Reduced Graphene Oxide as Highly-Active Bifunctional Electrocatalysts for Oxygen Reduction/Evolution Reactions. *ChemElectroChem*. **2016**, *3*, 1107–1115.

(11) Lee, D. U.; Kim, B. J.; Chen, Z. One-Pot Synthesis of a Mesoporous $NiCo_2O_4$ Nanoplatelet and Graphene Hybrid and Its Oxygen Reduction and Evolution Activities as an Efficient Bi-Functional Electrocatalyst. *J. Mater. Chem. A* **2013**, *1*, 4754.

(12) Liu, Q.; Jin, J.; Zhang, J. $NiCo_2S_4$@graphene as a Bifunctional Electrocatalyst for Oxygen Reduction and Evolution Reactions. *ACS Appl. Mater. Interfaces* **2013**, *5*, 5002–5008.

(13) Bian, W.; Yang, Z.; Strasser, P.; Yang, R. A $CoFe_2O_4$/Graphene Nanohybrid as an Efficient Bi-Functional Electrocatalyst for Oxygen Reduction and Oxygen Evolution. *J. Power Sources* **2014**, *250*, 196–203.

(14) Prabu, M.; Ramakrishnan, P.; Shanmugam, S. $CoMn_2O_4$ Nanoparticles Anchored on Nitrogen-Doped Graphene Nanosheets as Bifunctional Electrocatalyst for Rechargeable Zinc-Air Battery. *Electrochem. Commun.* **2014**, *41*, 59–63.

(15) Hardin, W. G.; Slanac, D. A.; Wang, X.; Dai, S.; Johnston, K. P.; Stevenson, K. J.

Highly Active, Nonprecious Metal Perovskite Electrocatalysts for Bifunctional Metal-Air Battery Electrodes. *J. Phys. Chem. Lett.* **2013**, *4*, 1254–1259.